


Physicochemical mechanisms of FT-NIRS age prediction in fish otoliths

Michelle S. Passerotti^{A,B,*} , Marcel J. M. Reichert^C, Bailey A. Robertory^{A,D}, Zachary Marsh^E, Morgan Stefik^E and Joseph M. Quattro^F

For full list of author affiliations and declarations see end of paper

***Correspondence to:**

Michelle S. Passerotti
NOAA Fisheries Apex Predators Program,
28 Tarzwell Drive, Narragansett,
RI 02884, USA
Email: michelle.passerotti@noaa.gov

Handling Editor:
Christine Dudgeon

Received: 2 December 2021

Accepted: 18 March 2022

Published: 10 May 2022

Cite this:

Passerotti MS *et al.* (2022)
Marine and Freshwater Research, **73**(6),
846–865.
doi:[10.1071/MF21341](https://doi.org/10.1071/MF21341)

© 2022 The Author(s) (or their employer(s)). Published by CSIRO Publishing.

ABSTRACT

Context. Fourier transform near-infrared spectroscopy (FT-NIRS) is of interest to fisheries managers for rapid age prediction in fish otoliths, yet the underlying prediction mechanism is unknown. **Aims.** To better understand drivers of FT-NIRS age prediction, we evaluated FT-NIRS spectra and age prediction models for otoliths of red snapper, *Lutjanus campechanus*, related to otolith structure, mass, and constituents (calcium carbonate (CaCO₃) and protein). **Methods.** Spectra were collected from a set of whole otoliths ($n = 84$, 0–28 years) and again sequentially after grinding to powder and subsampling a fixed mass of each ground otolith. Protein content was also measured ($n = 26$) and related to spectra. **Key results.** Age prediction was diminished in ground and fixed-mass otolith models, but remained within 2 years of traditional ages. Protein content (0.43–0.92% weight) increased significantly with age, implying a concomitant decrease in CaCO₃ content. FT-NIRS models predicted protein content to within 0.04%, but protein variability hindered modelling. Spectral characteristics of both CaCO₃ and protein are evident in otolith spectra and are implicated in age-prediction models. **Conclusions.** Changes in otolith composition, mass, and structure underlie FT-NIRS age prediction, but compositional changes inform the majority of age prediction. **Implications.** These results provide a foundation for understanding FT-NIRS age prediction.

Keywords: age estimation, fisheries management, *Lutjanus campechanus*, otolith chemistry, organic matter, protein, red snapper, spectroscopy.

Introduction

Fourier transform near infrared spectroscopy (FT-NIRS) has gained attention in the fisheries management community as a potential alternative to costly age estimation of fish, which traditionally relies on visual counts of growth bands in otoliths to estimate age (e.g. Campana 2001). Rapid, non-destructive scans of otoliths using FT-NIRS and subsequent regression modelling of spectral data with traditional age-calibration data has resulted in age predictions deemed mostly equivalent, from an experimental standpoint, to traditional estimates for both daily and annual ages across various species (Wedding *et al.* 2014; Robins *et al.* 2015; Helser *et al.* 2019; Passerotti *et al.* 2020a, 2020b; Healy *et al.* 2021; Wright *et al.* 2021). The case has also been made that FT-NIRS has potential to be useful in ecological studies, including discrimination of geographical differences manifested in otolith chemistry (e.g. Wedding *et al.* 2014; Robins *et al.* 2015), among other potential fisheries applications.

Studies have provided little empirical evidence of the chemical or structural basis for FT-NIRS age prediction in fish. Wedding *et al.* (2014) found that carbonate ion signatures were apparent in spectral data underlying otolith age calibrations, and Robins *et al.* (2015) hypothesised that water chemistry influences otolith spectral signatures because of changes in trace element concentrations across the lifespan. Helser *et al.* (2019) alternatively suggested that age-related changes in the otolith organic matrix underlie FT-NIRS age prediction based on spectral regions used in walleye

pollock age-prediction models. Similar regions were also implicated in age-prediction models for red snapper (Passerotti *et al.* 2020a, 2020b). Besides otoliths, mechanisms relating to the relative concentrations of mineral and organic constituents were also suggested as underlying FT-NIRS age prediction in elasmobranch tissues (Rigby *et al.* 2014, 2016, 2019). No direct measurements of otolith constituent composition have been related to FT-NIRS age predictions.

Most sagittal otoliths are generally thought to comprise calcium carbonate (CaCO_3 , $\geq 90\%$), organic matrix (proteins, collagens, and proteoglycans, $\leq 10\%$), and trace elements ($\leq 1\%$) (Campana 1999; Payan *et al.* 1999; Borelli *et al.* 2001; Chang and Geffen 2013), but composition is species-specific (e.g. Degens *et al.* 1969; Dauphin and Dufour 2003) and incompletely described for most species, particularly in regard to the organic matrix. Past studies have identified age-related differences in both organic and inorganic (i.e. mineral) otolith constituents, suggesting that otolith cores are more proteinaceous than are subsequent growth bands (Jolivet *et al.* 2008, 2013), that relative protein content declines with age in some species (e.g. Morales-Nin 1986a, 1986b), and that the ratio of water-soluble to water-insoluble proteins can vary across lifespan (Hoff and Fuiman 1993; Hüsey *et al.* 2004).

More recently, advances in the fields of proteomics and elemental chemistry have enabled both large-scale identification of otolith proteins and a more complete elucidation of the biomineralisation process. Thomas *et al.* (2019) used proteomics to detect more than 300 proteins in otoliths of black bream, *Acanthopagrus butcheri*, that were previously unknown to occur in otoliths, and Thomas *et al.* (2020) characterised the 3-D protein scaffolding in salmon, *Salmo salar*, otoliths, allowing novel characterisation of proteins, collagens, and enzymes, and tracing their dynamic role in biomineralisation across the lifespan of the fish. Recent work by Hüsey *et al.* (2021a) further described trace element patterns in otoliths across lifespans and showed their role in both mineral and organic portions of the otolith. Taken together, these studies have shown a highly complex biomineralisation process (briefly summarised below) in which both mineral and organic matrices vary not only with species and age, but also spatially across the otolith. These factors have major implications for age prediction by using FT-NIRS.

During otolith formation, collagens and collagen-like proteins (sometimes referred to as water-insoluble proteins) form the majority of the otolith organic template, including a large role of otolin-1, a collagen-like protein unique to otoliths that putatively forms the basis of the organic matrix on which CaCO_3 is precipitated (Degens *et al.* 1969; Dunkelberger *et al.* 1980; Davis *et al.* 1995; Murayama *et al.* 2002; Thomas *et al.* 2019). The daily alternating deposition of organic matrix and CaCO_3 forms the concentric growth bands associated with age estimation, a process governed by the other non-collagenous (i.e. water

soluble) regulatory proteins which are either deposited within the otolith matrix or entrained into interstitial spaces during otolith accretion (Thomas and Swearer 2019; Thomas *et al.* 2019; Hüsey *et al.* 2021b). The mechanism for accretion of material from the saccular epithelium creates gradients in the endolymph fluid that can also translate to corresponding protein gradients along the accretion axis, in turn creating cyclic changes in composition, density, and opacity (e.g. Hoff and Fuiman 1993; Hüsey *et al.* 2004; Thomas *et al.* 2020). There is also heterogeneity in elemental distribution patterns (Izzo *et al.* 2016; Limburg and Elfman 2017; Hüsey *et al.* 2021b), although it is unclear whether FT-NIRS detects elemental differences at the concentrations (low parts per million) present in otoliths. Hence, spatial heterogeneity in otolith chemistry can be present owing to both age and the physical mechanisms of otolith accretion.

Beyond chemical composition, additional questions surround the relationship of FT-NIRS with physical attributes such as otolith size. Robins *et al.* (2015) compared ages predicted from direct regressions of otolith weight with age with those of FT-NIRS prediction models and found that FT-NIRS models were more accurate, concluding that FT-NIRS cannot be solely reliant on otolith weight for informing age prediction. Passerotti *et al.* (2020a) found that FT-NIRS models predicted otolith weight better than they predicted age based on partial least-square (PLS) model metrics, but that different spectral signatures were responsible for the two models. However, Passerotti *et al.* (2020b) found that light penetration was attenuated in older, larger, and thicker red snapper otoliths, potentially hindering accurate age prediction in older individuals of this species. This also has implications for how physical light interaction with the otolith (i.e. sample presentation) affects age prediction. NIR light is known to penetrate substrates more deeply than are other types of infrared light (up to 10 cm; Workman and Weyer 2012), but this is highly dependent on the physical and chemical makeup of the substance and varies according to wavenumber region (Workman and Weyer 2012; Williams 2019). The ability to detect chemical signatures under the surface layers of the otolith is of paramount interest, given the structural heterogeneity of constituents and the unknown origins of FT-NIRS age prediction overall.

Defining the causation underlying FT-NIRS otolith age prediction is desirable, but linking causation to empirical analyte properties is difficult. The use of FT-NIRS for standardised predictive analyses requires the evaluation of critical key assumptions, namely that concentrations of components of interest are in some way related to the spectral data generated from the technique (Chen and Wang 2001). This is a daunting task, given that otoliths are composites of potentially many measurable, yet largely unknown, components. FT-NIRS is used in various industries such as agriculture and pharmaceuticals to passively monitor sample composition for constituents of interest, such as, for example, protein content

(e.g. Williams *et al.* 1985). Assigning specific features of NIR signatures to individual constituents is not always possible, and often multiple similar constituents, such as different types of proteins, are grouped together and detected using combination bands found to correlate with the overall content of broader constituent categories (Workman and Weyer 2012). Hence, preliminary evaluation of the constituent changes underlying otolith age prediction with FT-NIRS logically begins with attribution of broad constituent groupings, i.e. mineral/inorganic and protein/organic components, with age-specific otolith spectral signatures. Further correlation of age model regression coefficients with wavenumber regions attributable to constituent groups would further help define the relationship, if only superficially.

Towards this end, our goal was to explore the relationship of primary otolith constituents (CaCO₃ and protein), otolith size (sample mass), and otolith structure (whole and ground) to FT-NIRS spectra and age prediction in pursuit of an improved, albeit basic, understanding of the NIR spectral correlation with age in fish otoliths. To accomplish this, we first compared spectral signatures of CaCO₃ and Type I collagen with otolith spectra to identify likely areas of contribution of mineral and organic fractions respectively, to otolith spectral signatures. We then conducted experiments to compare FT-NIRS spectra and age prediction across various preparations of the same otolith set, including (1) whole, intact otoliths per other FT-NIRS studies, (2) the same otoliths after grinding to powder (hence removing the effects of shape and structure), and (3) a fixed-mass subsample of each powdered otolith (hence removing the effect of sample mass). We also simulated otolith accretion by using pure CaCO₃ to test the influence of an increasing sample mass, but not constituent concentration, on age prediction (hence simulating a change in size but not 'age'). Finally, otolith protein content was quantified, correlated with age, and the FT-NIRS prediction capability was evaluated to determine whether changing protein content underlies FT-NIRS age prediction in otoliths.

Materials and methods

Otolith collection and age estimation

Red snapper otoliths were sourced from archival fishery-independent collections taken from the south-eastern US Atlantic Ocean by the South Carolina Department of Natural Resources (SCDNR), Marine Resources Research Institute, as part of the South-east Reef Fish Survey and Marine Resources Monitoring Assessment and Prediction (MARMAP) sampling program between 2011 and 2016. Generally, left otoliths were sectioned for ageing, leaving the right otolith available for FT-NIRS. A traditional calendar age estimate was generated from the left otolith by using methods outlined in Wyanski *et al.* (2015). These 'traditional' ages were used as

reference values to inform FT-NIRS age-prediction models as well as for other age-correlation models in this study. The paired right otoliths corresponding to these ages were used for the subsequent analyses below.

Spectral comparison of otoliths and constituents

To explore the relationship of the mineral and organic fractions of otolith composition with the red snapper otolith FT-NIRS spectral signature, we visually compared a spectrum from a whole red snapper otolith with those of other analytes representative of the two fractions. The mineral portion was modelled using powdered CaCO₃ in the form of precipitated calcite (Amresco, CAS# 471-34-1), and the organic portion was modelled using a Type I collagen signature described in Kandel *et al.* (2020). In addition, we compared individual vibrational mode peak assignments mapped by Hopkinson *et al.* (2017) for CaCO₃, which are driven by the activity of the CO₃²⁻ anion and hence O–H bond signatures, to help visualise the complexity of the molecular interactions underlying the relatively broad NIR signatures of composite materials. Alignment of peaks underlying the CaCO₃ signature with perceived features in the otolith signature were considered to represent areas of mineral influence, and those aligned with the Type I collagen signature were considered to represent areas of organic influence, with the understanding that there are numerous additional and potentially unknowable molecules present in otoliths that could also influence the NIR signature. The form of CaCO₃ in otoliths is typically aragonite, but calcite is used here for comparison because it is commercially available in purified form and, in comparison, presents only minor variations in NIR signature (Gaffey 1987; Hopkinson and Rutt 2016). However, we did test for consistency of aragonite as the predominant CaCO₃ polymorph across red snapper otoliths of different ages and ruled out any effect of changing polymorph on spectral comparisons. The methods and results for this analysis can be found in Supplementary materials.

Sample structure and sample mass experiments

A set of 84 otoliths ranging in age from 0 to 28 years was selected for evaluation of the effects of sample structure (whole vs ground) and sample mass on FT-NIRS spectral signatures and age prediction. Structure and mass experiments are further described below. Otoliths were stored dry in paper coin envelopes under ambient conditions from time of collection to the time of experiments. Differences in the time elapsed since collection can affect spectral signatures, potentially owing to moisture content (Robins *et al.* 2015); hence, before structure and mass experiments, otoliths were dried at 55°C for 24 h in a sealed oven containing an excess of desiccant. After 24 h, otoliths were allowed to come to room temperature inside the oven, and were then individually removed immediately before FT-NIRS scanning

as outlined below. After scanning, otoliths were weighed to the nearest 0.001 mg on a Mettler Toledo microbalance.

Sample structure: grinding experiment

After drying, the 84 otoliths were individually ground to powder with a tungsten-carbide ring mill until the entire sample easily passed through a 250-micron sieve. Grinding time was standardised among samples to help ensure uniform particle size, and the ring mill was thoroughly cleaned between samples to avoid cross-contamination. The full mass of each powdered otolith was loaded into a 22 mm cylindrical borosilicate glass cuvette and scanned as described below. Spectral signatures and FT-NIRS age prediction were evaluated and compared with that of whole intact otoliths on the basis of differences in PLS regression parameters.

Sample mass: fixed-mass experiment

Following scanning of the full volumes of ground otoliths, a 300 mg subsample was taken from each ground otolith to comprise fixed-mass ground (FMG) samples of each. Only otoliths aged ≥ 3 years were included in the fixed-mass analysis ($n = 71$), because most of the otoliths aged 0–2 years were smaller than 300 mg. Each FMG sample was placed into a clean cuvette and scanned in an identical manner to the full ground otoliths. Spectral signatures and FT-NIRS age prediction were evaluated and compared with those of intact and ground otoliths on the basis of differences in PLS regression parameters.

Simulated CaCO₃ accretion

To evaluate the effects on age prediction of increasing sample mass without associated increases in analyte (i.e. age-related organic compound) concentration, powdered CaCO₃ (Amresco, CAS# 471-34-1) was scanned in quantities ranging from 100 to 1000 mg in 100 mg intervals. Spectra were collected as for otolith powders as outlined below. To model the effect of increasing otolith mass on age prediction, each quantity of CaCO₃ powder was assigned a dummy variable of 'layer age', ranging in value from 1 to 10 years according to its sample mass (e.g. 100 mg = 1 year old, 200 mg = 2 years old) and three replicates of each mass were scanned for a total of $n = 30$ data points. An age-prediction model was created using PLS regression as described for otoliths above, and resulting regression parameters were evaluated for goodness of fit. Optimised wavenumber regions, regression coefficients, and factor loadings for the CaCO₃ 'layer age' model were compared with those from otoliths in all preparations to infer signatures related to mineral CaCO₃ content and increasing sample mass in the absence of otolith organic components.

Protein/amino acid content

To examine the relationship between protein content and FT-NIRS age prediction in otoliths, acid-hydrolysed amino acid content was measured and used to estimate total protein content in $n = 26$ otoliths ranging in age from 0 to 25 years. Subsamples of ground otoliths for which spectral data were previously collected as above were analysed for amino acid content at the Molecular Structure Facility, University of California, Davis Genome Centre (Davis, CA), by using the acid hydrolysis and post-column ninhydrin detection methods described in Cooper *et al.* (2000). Protein content for each otolith was calculated by summing the total AA residues quantified for each sample, after correction for recovery of standards analysed simultaneously with otolith samples (average correction = 1.9%). During acid hydrolysis, asparagine and glutamine are converted to aspartic (ASX) and glutamic acid (GLX) respectively; hence, the reported totals for ASX and GLX reflect these combined values.

To evaluate the ability of FT-NIRS to detect and predict protein content from otoliths, PLS regressions were fit to spectral data from all otolith preparations and related to protein content as measured above. Data preprocessing was performed as noted for age-prediction models below, and optimisation was performed to identify best-fit protein-prediction models. Optimised wavenumber regions, regression coefficients, and factor loadings for protein-prediction models were compared with those from otoliths in all preparations and CaCO₃ models to identify spectral signatures unique to otolith protein content. Changes to individual amino acid concentration (% otolith weight) were plotted graphically as a function of age, and linear trends were evaluated by calculating Pearson product-moment correlation coefficients for each. All regressions and associated analyses were performed using R (ver. 3.4.3 'kite-eating tree', 2017).

FT-NIRS data collection/analysis

FT-NIR spectral data for samples in all preparations (whole intact otoliths, whole ground otoliths, fixed-mass subsamples of ground otoliths (FMG), and powdered CaCO₃) were collected using a Bruker Matrix-I FT-NIR spectrometer (Bruker Scientific, Billerica, MA, USA). Samples were positioned on the sample window according to their preparation. Whole intact otoliths were scanned by placing them directly on the centre of the sample window, convex side down, positioned so that the rostral axis of the otolith was horizontal in relation to the sample window (e.g. Robins *et al.* 2015). Powdered samples were loaded into individual 22 mm cylindrical borosilicate glass cuvettes and placed onto the sample window with a microsample collar (Bruker Scientific) fitted to the sample window. In total, 64 spectral scans were acquired for each sample at a frequency of 16 cm⁻¹ along the

entire NIR spectrum (3600–12 000 cm^{-1}) and averaged to produce a single representative spectrogram for each sample in each presentation.

Spectral data analysis was conducted using the OPUS software suite (ver. 7.8; Bruker Scientific, Billerica, MA, USA). Spectral data were fitted to traditional otolith ages and protein concentrations by using PLS regression (Chen and Wang 2001). Calibration models were evaluated for prediction capability using a 'leave one out' method of cross-validation, and goodness of fit was judged on the basis of the coefficient of determination (R^2), root mean square error of cross-validation (RMSECV), and residual prediction deviation (RPD; a ratio of the standard deviation to the standard error of prediction). The RMSECV metric was minimised, the R^2 maximised, and RPD was ≥ 3 and maximised to be considered optimal (Williams 2019). Because of small sample sizes ($n \leq 84$) for each of our experiments, only calibration models were evaluated because splitting samples into separate smaller calibration and validation sample sets might promote over-confidence in validation models (Williams 2013).

For our purposes, otolith age-prediction models for each experimental treatment group were constructed in the following two forms: (1) 'standardised' models used a standardised wavenumber range of 6104–4200 cm^{-1} to facilitate comparison based on important wavenumber regions for predicting age in previous publications (Passerotti *et al.* 2020a, 2020b); and (2) 'optimised' models in which wavenumber regions were optimised to fit the unique dataset and treatments applied in this study to facilitate identification of potentially unique spectral features arising from these variables. The same process was also used to fit PLS regressions for predicting otolith protein content and calcium carbonate 'layer age' as described above.

Preprocessing for all otolith models except the FMG models consisted of a Savitzky–Golay first derivative transformation with 17 smoothing points (polynomial order = 2), whereas FMG models also underwent vector normalisation using the standard normal variate (SNV) function in addition to the Savitzky–Golay transform. Calcium carbonate signatures were also preprocessed using Savitzky–Golay transformation and SNV. Savitzky–Golay transformation is typically used to correct for baseline shifts owing to light scatter from differences in particle size and/or other physical differences among samples, whereas SNV normalises the data to a mean of 0 and standard deviation of 1. Analyses of absorbance patterns at specific wavelengths were performed using preprocessed data for consistency with age-prediction models; given that all spectra were subject to first derivative transformation, this means that changes associated with peaks in raw spectral data will be offset to either side of the original peak in the transformed data. Hence, changes to specific features in absorbance patterns, e.g. collagen features, were evaluated across a small range of nearby

wavenumbers and denoted with approximate wavenumber location.

Results

Spectral comparison

Comparison of representative spectral signatures from CaCO_3 and Type I collagen identified features from each that potentially contribute to the otolith signature, and curve deconvolution for the CaCO_3 signature from Hopkinson *et al.* (2017) provides additional insight into the underlying vibrational modes of the CO_3^{2-} anion contributing to the overall shape of the CaCO_3 and, potentially, the otolith spectrum (Fig. 1). In the raw otolith signature, water features near 6840 cm^{-1} and 5160 cm^{-1} are evident as identified previously for otoliths in Gauldie *et al.* (1998), and similar but broader, more flattened peaks are apparent in the collagen signature. These peaks are notably absent from the CaCO_3 signature, which instead contains a smaller peak near 7200 cm^{-1} and narrow peaks near 5334 cm^{-1} and 5008 cm^{-1} . Additional CaCO_3 peaks near 4630 cm^{-1} and 4501 cm^{-1} are offset from any visible features in the otolith signature, but the most prominent CaCO_3 peak near 4268 cm^{-1} aligns with the leading edge of the broader otolith peak near 4310 cm^{-1} . This broader peak might also be influenced by the CaCO_3 peak at 4346 cm^{-1} . Collagen features that align with those in the otolith signature occur near 5924 cm^{-1} and 5778 cm^{-1} , corresponding to known methyl ($-\text{CH}_3$) and methylene ($-\text{CH}_2$) group vibrations respectively (Workman and Weyer 2012), as well as smaller peaks near 4898 cm^{-1} and 4596 cm^{-1} .

Grinding experiment

Raw absorbance signatures of ground otoliths were similar to those of intact otoliths, but absorbance was lower overall with apparently reduced effects of light scattering and baseline drift (i.e. the 'fanning' effect in spectra across age groups in whole otoliths; Fig. 2a, b). The relative magnitude of individual spectral features also appears somewhat reduced or flattened, such as, for example, the $-\text{OH}$ overtone peak near 6900 cm^{-1} and smaller features between 4600 and 5000 cm^{-1} . Preprocessed absorbance signatures were also similar in shape to those of intact otoliths (Fig. 3a, b), but differences in signatures of ground Age-0 otoliths are much more apparent than in intact otoliths, especially near 7200 cm^{-1} and ~ 4600 – 4500 cm^{-1} .

Ages predicted with the standardised model were less accurate for ground otoliths than intact otoliths on the basis of RMSECV (Table 1, Fig. 4), with more deviation in the youngest and oldest ages and in a more non-linear pattern. Nonetheless, the ground otolith standardised model approached an RPD of 3 and R^2 of 0.88, and the optimised

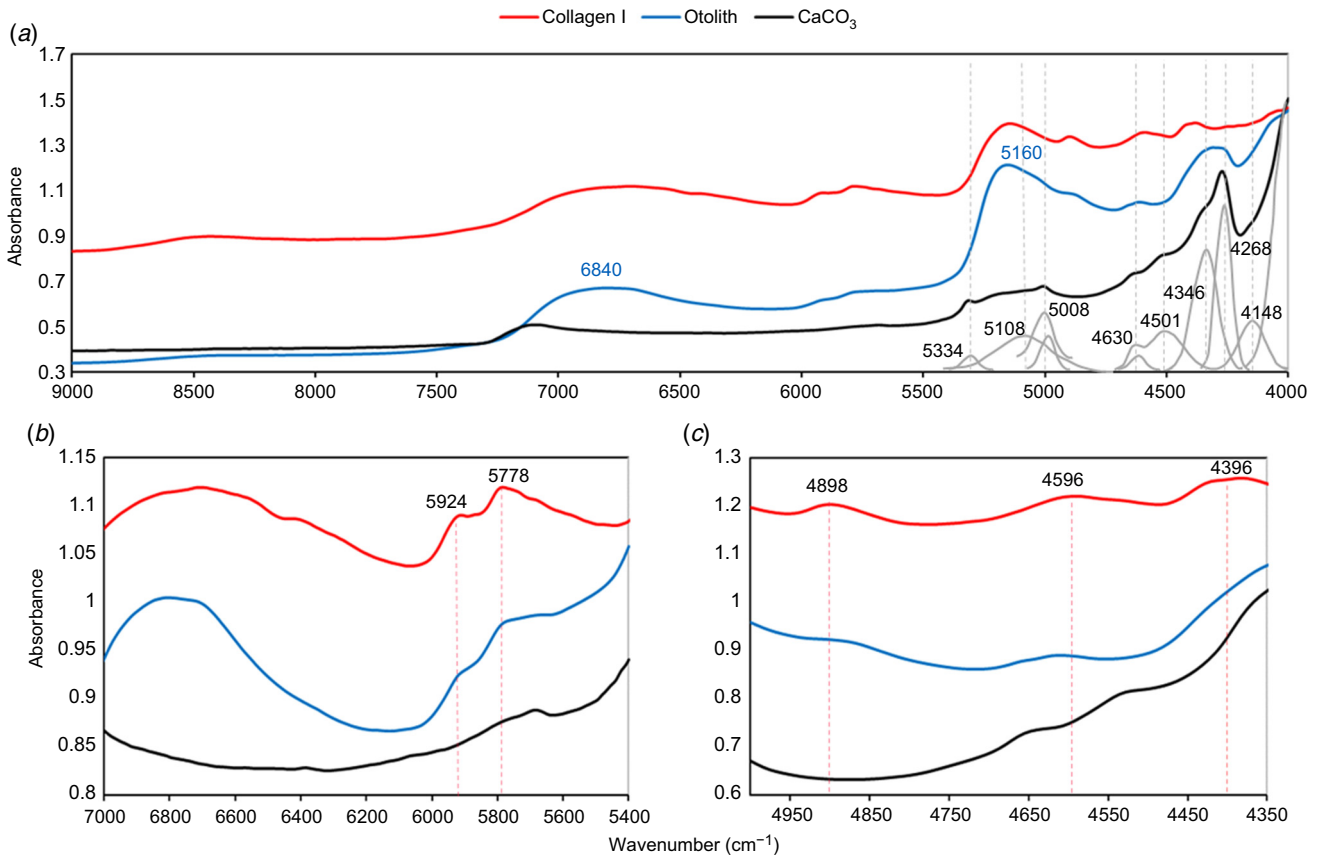


Fig. 1. Comparison of NIR spectral signatures from powdered Type I collagen (Kandel *et al.* 2020), whole intact red snapper otolith (age = 16 years), and powdered calcium carbonate. In *a*, resolved CaCO_3 band contributions from respective vibrational modes are represented with grey curves (from Hopkinson *et al.* 2017) and grey dashed lines are given to visualise alignment of deconvolved CaCO_3 peaks with other spectra. Numbered peaks in the otolith spectrum denote water features as described by Gaudie *et al.* (1998). In *b* and *c*, subsets of the spectral range containing known collagen peak assignments (numbered) are shown, with red dashed lines given to visualise alignment of collagen peaks to the otolith spectrum.

model, which overlapped intact otolith optimised regions and added the region at $\sim 7450\text{--}6770\text{ cm}^{-1}$, improved to an RPD of 3.15 and R^2 of ~ 0.90 . Regression coefficients were similar between the whole-ground and whole-intact models for the regions near 5800 cm^{-1} and $5200\text{--}4900\text{ cm}^{-1}$; all other peaks occurred at similar locations but were of opposite direction (Fig. 5a). On the basis of comparisons of transformed spectra in Fig. 3, these differences could stem from broadening of absorbance peaks in ground spectra, which would shift the inflection points highlighted in the transformed spectra and, hence, the regression coefficients.

Fixed-mass experiment

Raw absorbance signatures of fixed-mass ground (FMG) otolith samples were similar in pattern but were relatively flattened and with fewer prominent features than for the other otolith preparations (Fig. 2c). Preprocessed spectra were likewise similar in shape to those from the other otolith

preparations but with far less variation in magnitude among age groups as evidenced by spacing of absorbance values under peak curves (Fig. 3c).

Age-prediction models for FMG samples had diminished resolution relative to those from other preparations and the models became more non-linear (Table 1, Fig. 4), but age was nonetheless predictable from fixed-mass samples and, hence, not reliant on otolith size or structure to inform age models. Standardised region models had the lowest R^2 and RPD of all the age models, but also used fewer factors (rank = 3) to explain the age relationship, with Factor 1 explaining $\sim 67\%$ of the spectral variance (Fig. 6). The optimised model performed well relative to other published FT-NIRS age prediction models, predicting age to within ~ 2 years and with RPD of >3 . In the optimised model, the number of explanatory factors increased to $n = 8$, but the variance explained by Factor 1 was the highest of all models at 79%. Regression coefficients for FMG samples generally followed the

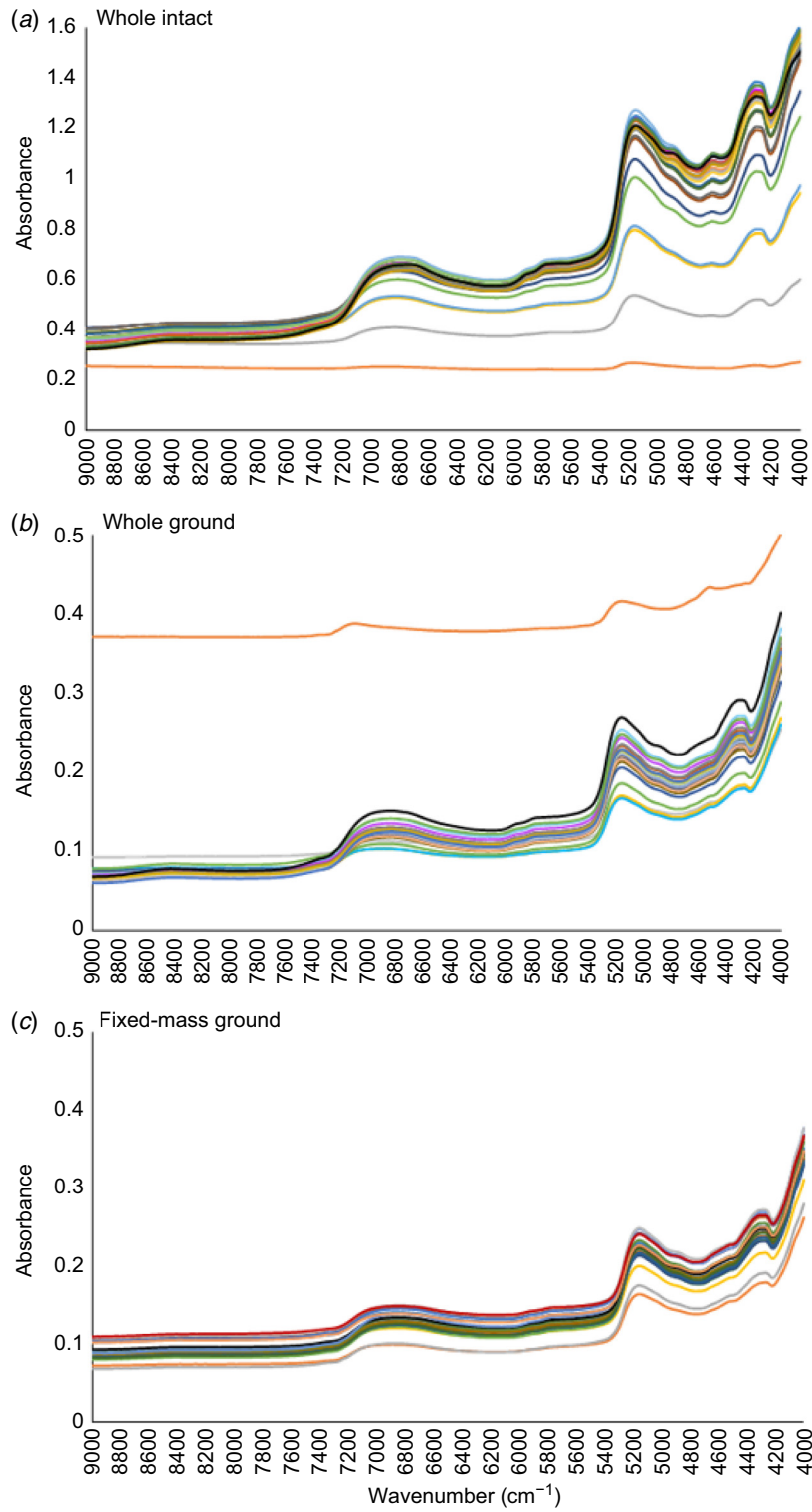
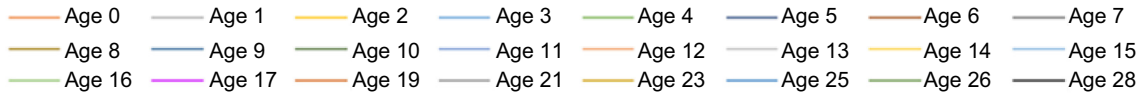


Fig. 2. FT-NIR spectral signatures for red snapper otoliths in (a) whole intact, (b) whole ground, and (c) fixed-mass ground preparations, averaged by age.

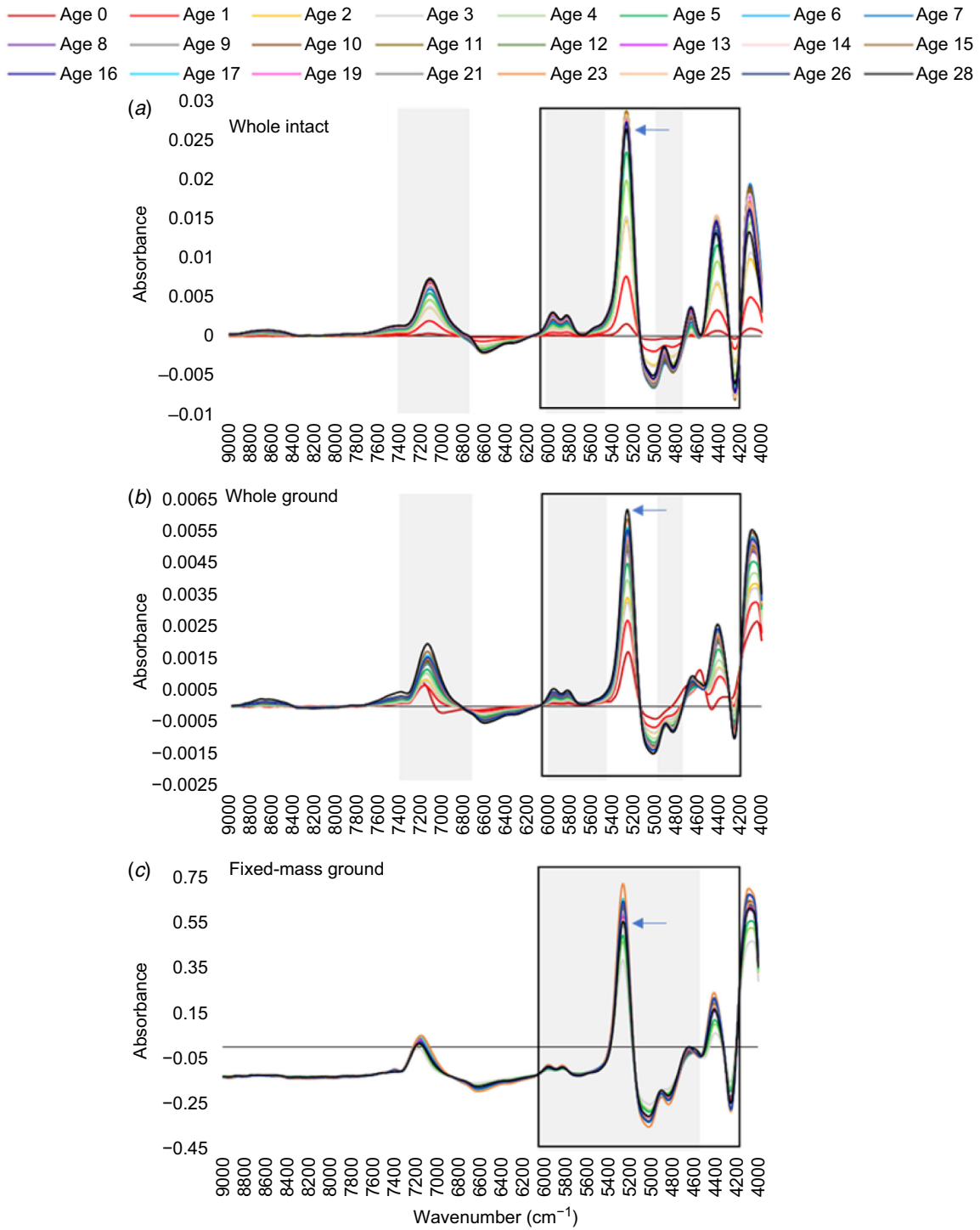


Fig. 3. Red snapper otolith (a, b) first-derivative and (c) first-derivative + SNV preprocessed FT-NIRS spectra, averaged by age, for each sample treatment. Arrows denote the absorbance value of the oldest otolith (age = 28 years) near 5200 cm^{-1} , for reference. Fixed-mass ground samples did not include ages <3 years. Black boxes delineate the wavenumber regions included in the standardised age-prediction models, and grey shading delineates wavenumber regions included in optimised age-prediction models.

Table 1. PLS prediction model results for red snapper otolith age and calcium carbonate 'layer age' regressions.

Model	<i>n</i>	Wavenumber region(s)	<i>R</i> ²	RMSECV	RPD	Bias	Rank
Whole intact, standardised	84	6104–4200	93.8	1.71	4.03	−0.014	5
Whole intact, optimised	84	7456–6768	94.4	1.62	4.23	−0.016	4
		6032–5496					
		4952–4768					
Whole ground, standardised	84	6104–4200	88.0	2.38	2.89	−0.013	4
Whole ground, optimised	84	7456–6768	89.9	2.19	3.15	−0.011	5
		6032–5496					
		4952–4768					
Fixed-mass ground, standardised	71	6104–4200	83.4	2.48	2.45	0.047	3
Fixed-mass ground, optimised	71	6104–4544	89.0	2.02	3.02	0.033	8
Powdered CaCO ₃ , standardised	30	6104–4200	87.4	1.02	2.82	0.008	5
Powdered CaCO ₃ , optimised	30	6104–4600	90.7	0.878	3.27	0.009	5

patterns of whole-ground otoliths but with minor changes in magnitude near 6000–5800 cm^{−1}, 5150 cm^{−1}, and 4700–4300 cm^{−1} (Fig. 5b). Peak shifting was also evident near 5300 cm^{−1} and 4550 cm^{−1}. Hence, grinding appears to have had the largest overall effect on regression coefficients across all otolith treatments, ostensibly because of the changes in the interaction of NIR light with whole intact otoliths relative to ground otoliths.

Simulated CaCO₃ accretion

Layering of powdered CaCO₃ resulted in predictable 'layer age' by using a PLS regression model (Table 1, Fig. 7), despite preprocessing of spectral data, which is generally used to remove effects from physical variations in samples occurring secondarily to the primary analyte of interest (Rinnan et al. 2009). Preprocessed spectra for 'layer ages' highlighted features of interest for comparison with otoliths, including the absence of prominent peaks between ~5960 and 5700 cm^{−1}, the less prominent but more numerous features in the 5400–5000 cm^{−1} range, and the two small peaks near 4600 and 4500 cm^{−1} that lead up to the prominent peak near 4300 cm^{−1}, which is much narrower than that seen in otoliths (Fig. 7). Layer-age models predicted increasing sample mass/thickness in the standardised region to within one layer (RMSECV = 1 or 100 mg sample mass), and with an RPD approaching 3. When optimised for wavenumber region, RMSECV declined to <1 with RPD of >3, and wavenumber region 6104–4600 cm^{−1}. Regression coefficients for the layer-age standardised model differed from ground-otolith age patterns in distinctive ways (Fig. 5c). Primarily, the regression coefficient pattern consisted of mostly broad features with few prominent, recognisable peaks, and did not follow otolith age coefficients in any predictable manner. Some regions exhibited similarity such as those near

5850–5600 cm^{−1}, 5200–5050 cm^{−1}, and 4800–4600 cm^{−1}, but remaining regions were all of opposite magnitude for otolith age models relative to layer age. Hence, where regression coefficient patterns between these models overlap, we can hypothesise that the mineral component of the otolith composition is contributing to the otolith age model, and where coefficients do not coincide or differ in direction, other factors, e.g. organic constituents might be more influential.

Protein/amino acid content

Protein comprised a small proportion of red snapper otoliths, ranging from 0.43 to 0.92% composition by weight, and protein concentration increased linearly with age (*R*² = 0.651, *P* < 0.0001; Fig. 8). Corresponding amino acid (AA) concentrations (% otolith weight) were positively correlated with age in all cases (*r* ≥ 0.478, *P* ≤ 0.014), but individual variation was also apparent to varying degrees, depending on the AA (Fig. 9). As a proportion of total protein weight, AA-specific age-related trends are apparent and 9 of 15 were significantly correlated, suggesting the relative quantities and specific types of proteins present in otoliths vary significantly with age (Fig. 10).

Prediction of otolith protein concentration from spectral data was not as successful as that of age, and varied with otolith preparation (Table 2). Protein prediction using the standardised region model was poor (RPD = 1.58) and was only slightly improved by utilising the optimised region model (RPD = 1.76, Fig. 11). Protein concentrations for three otoliths stood out as outliers as identified in Fig. 12, and are also visibly distinct in several AA plots (e.g. PRO and GLY) in Fig. 9. In most protein-prediction models, one or more of these otoliths were identified as outliers *via* Mahalanobis distance calculations of spectral data and were consistently under-predicted by models, as indicated in

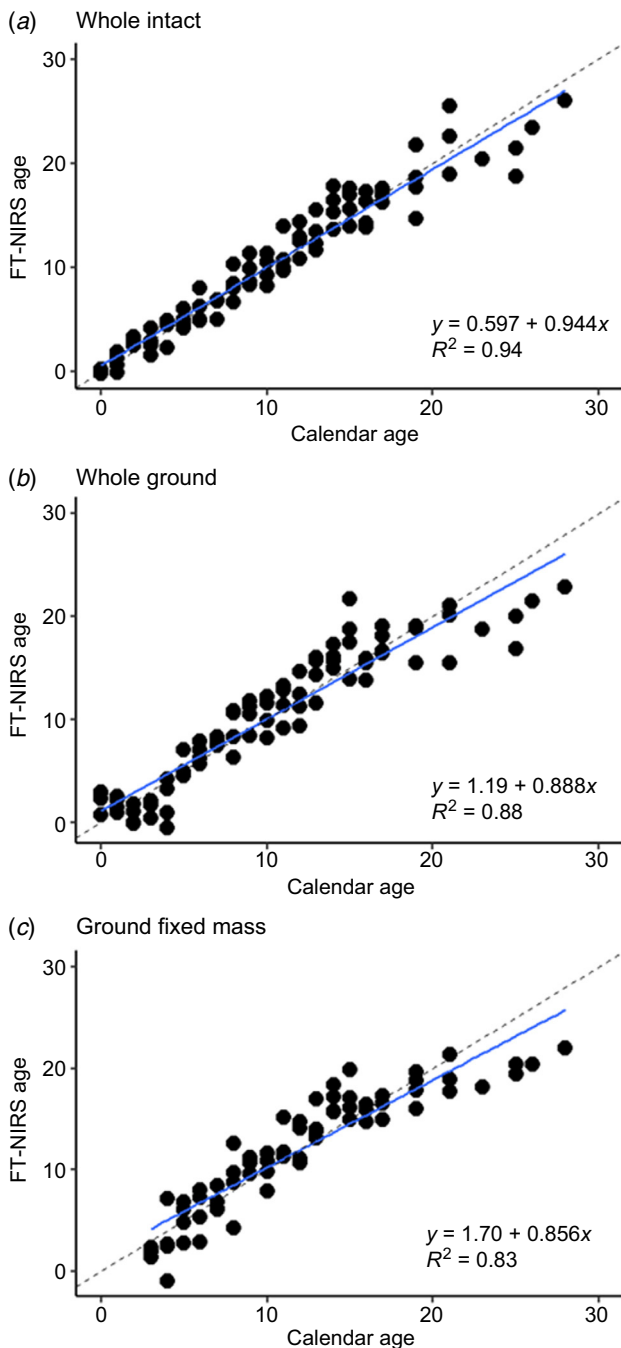


Fig. 4. Red snapper otolith PLS age regressions for 'standardised' region (6104–4200 cm^{-1}) models (solid lines) relative to a 1:1 relationship (dashed lines) on the basis of (a) whole intact, (b) whole ground and (c) fixed-mass ground otolith spectra.

Fig. 11a, c. Hence, these points were removed and prediction models recalculated (reduced models, Table 2, Fig. 11b, d). Reduced models were successful at predicting protein concentration to within $\sim 0.04\%$ in whole intact otoliths and $\sim 0.02\%$ in FMG samples. Wavenumber regions used in optimised protein-prediction models were narrow, focusing on 4688–4600 cm^{-1} in whole intact otoliths and 4600–

4544 cm^{-1} in FMG samples, which overlap with important regions for both FMG age-prediction models (Table 1). These regions are documented as useful for protein prediction (Workman 2001) and encompass various vibrations of N–H, C–N, and C=O bonds (Workman and Weyer 2012).

Protein-prediction models suggest that protein is detectable in intact and FMG otoliths by using FT-NIRS, but the low percentage composition and high variability with age make direct prediction challenging. Because protein concentration increased with age independently of sample mass in FMG samples, we can hypothesise that the CaCO_3 component, likewise, decreased in concentration with age. Because of its relatively higher concentration and ostensibly easier detection, correlation of CaCO_3 dynamics might be more easily modelled with age, which would manifest in negative correlation of regression coefficients at organic (i.e. collagen)-specific wavenumbers, or in positive correlation at CaCO_3 -specific wavenumbers. When coefficients were compared between the standardised CaCO_3 layer age and FMG otolith age models, most collagen-specific wavenumbers were positively correlated with age, including the 4688–4544 cm^{-1} region encompassing optimised protein-prediction models, whereas CaCO_3 -specific wavenumbers were not overtly influential (Fig. 5c). Although regression coefficients can be difficult to interpret when based on transformed data, this analysis solidifies the complementary relationship of these features with age and suggests that both mineral and organic signatures are used concordantly to predict age-related changes in percentage composition independent of sample mass.

Discussion

Typically, the first step in establishing a calibration model for spectroscopic prediction of an analyte is to identify all potential variables affecting the system under investigation (Beebe *et al.* 1998). In the case of fish otoliths, there are potentially hundreds of individual components comprising the structure itself, assuming individual organic matrix constituents (e.g. proteins, proteoglycans), trace elements, and the remaining mineral fraction act individually to alter the NIR signature. The various types of vibrations that each molecule within the constituents will undergo in the presence of NIR light, and how these molecules interact with all others, must also be considered (Siesler *et al.* 2002; Workman and Weyer 2012). The superficial comparison of the otolith spectral signature with that of individual constituents such as collagen and CaCO_3 is a first attempt to understanding the primary factors influencing FT-NIRS age prediction. NIR spectral signatures generally comprise broad, overlapping peaks in the combination and overtone regions of the NIR electromagnetic spectrum, which can be difficult to assign to specific chemical bond vibrational

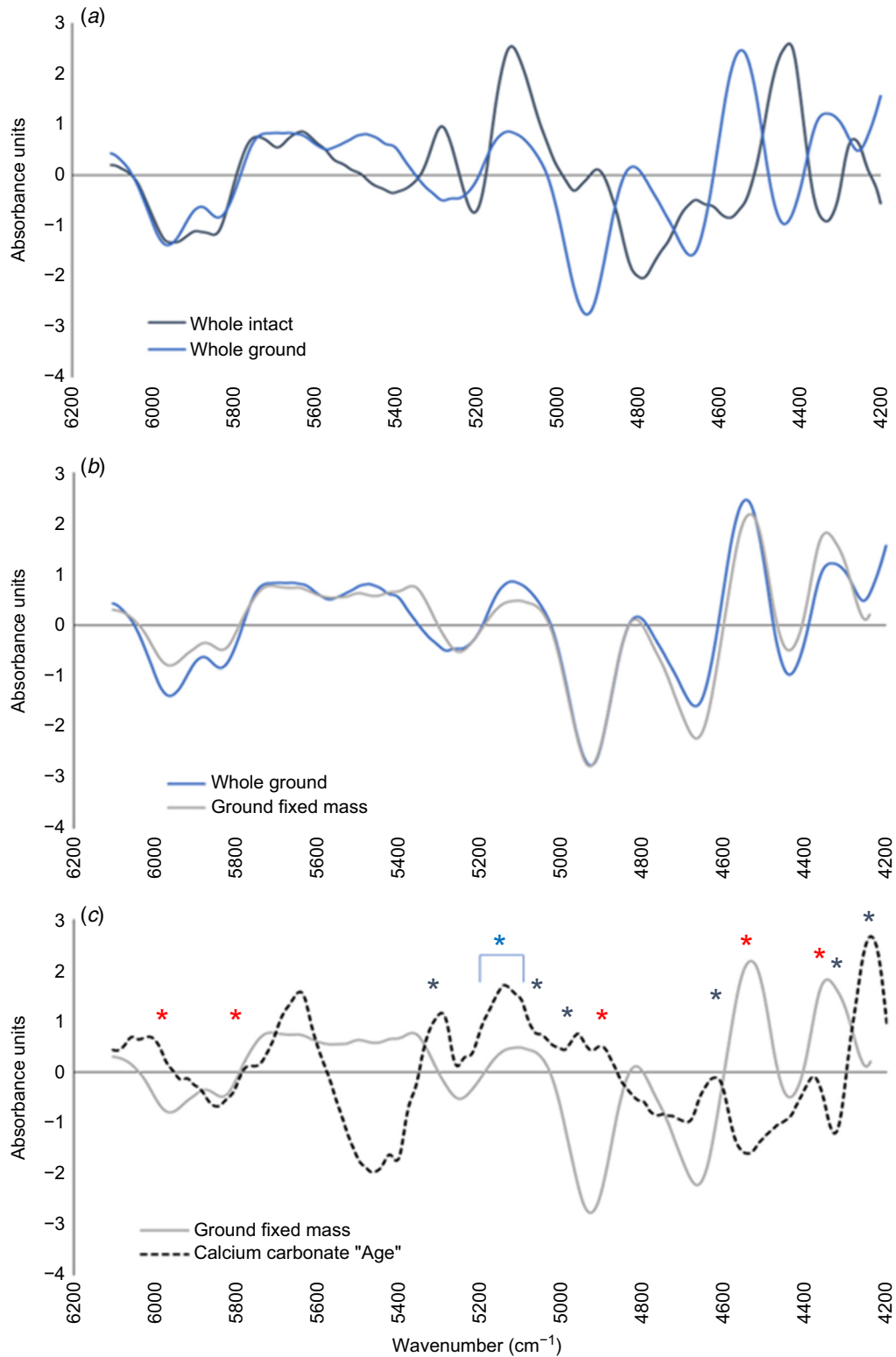


Fig. 5. Red snapper FT-NIRS PLS regression coefficients for ‘standardised’ region age models (6104–4200 cm^{-1}) comparing (a) whole intact and ground otoliths, (b) whole ground and fixed-mass subsamples of ground otoliths and (c) the calcium carbonate ‘layer-age’ treatment and fixed-mass subsamples of ground otoliths. All coefficients were standardised to Z scores to facilitate comparisons. In (c), coloured asterisks correspond to influential wavenumbers for collagen (red), CaCO_3 (grey) and water (blue) signatures as documented in Fig. 1.

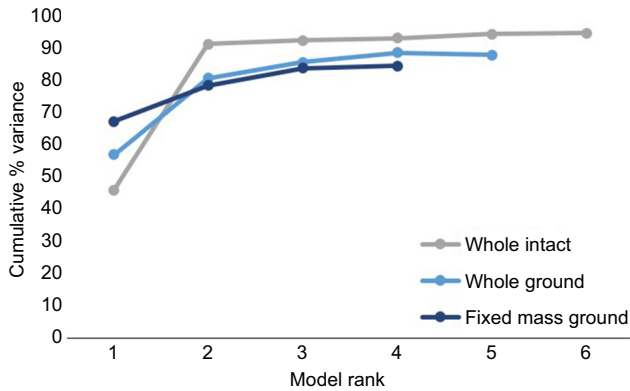


Fig. 6. Scree plot of ‘standardised’ age model variance explained per modelled rank (number of latent variables), for each of the otolith treatments.

modes even when all constituents are known at the molecular level (Alm *et al.* 2007; Workman and Weyer 2012). A telling visualisation is the number of individual peaks underlying the CaCO_3 signature presented herein (Fig. 1), which encompass at least seven features demonstrating characteristic types of vibrational modes stemming from a single carbonate ion (Hopkinson *et al.* 2017). With that in mind, we can then consider the complexity that must underlie the Type I collagen ($\text{C}_{65}\text{H}_{102}\text{N}_{18}\text{O}_{21}$) signature (Kandel *et al.* 2020), the full complement of vibrational modes for which, to our knowledge, have not been fully resolved in the literature. There are also necessary considerations for physical variables related to the otolith and its presentation to the NIR light, such as varying shape, particle size, specular reflection, opacity, and density (Workman and Weyer 2012), at least some of which are not constant within individual otoliths (e.g. growth bands of different composition and optical properties) nor across otoliths of different ages. To put it simply, it is complicated. Hence, the spectral-signature comparisons herein are not meant to be all-encompassing, but rather attempt to relate the basic relationship between mineral and organic fractions of the otolith to FT-NIRS age prediction, with the understanding that there are numerous other possibilities for constituents and physical interactions to shape the otolith spectral signature.

The results of this study have confirmed the ability of FT-NIRS to detect age-related chemical changes in otoliths, independent of concomitant changes in otolith size with age, and that these chemical changes do not arise from any systematic differences in crystal structure with age, although the random occurrence of atomic substitutions in the crystal lattice and any associated effect on FT-NIRS signatures cannot be addressed with the current data. However, some effects of physical changes, arising from the inherent characteristics of the whole otolith structure and how it changes with age, are evident in contributing to age prediction, and are important in understanding the impacts

of sample presentation for future FT-NIRS applications. Finally, otolith protein content and associated age-related amino acid dynamics reported herein provide insights into the complexities of the otolith organic matrix and its potential to inform FT-NIRS applications for age prediction and beyond.

Protein made up a small but measurable portion of red snapper otoliths by weight and was not well predicted from spectral signatures, without the removal of outliers to reduce sample-set variability. However, the positive correlation of protein concentration with age provides a potential chemical basis for age prediction beyond simple correlation of overall spectral absorbance with increased otolith size. To our knowledge, estimates of red snapper otolith total protein content are not published elsewhere. Lueders-Dumont *et al.* (2020) documented increasing intracrystalline nitrogen content with otolith weight in three red snapper otoliths (~600–1100-mg otolith weight, ~1–6 years old on the basis of otolith weight-at-age reported herein), but did not report total protein content. The adult otoliths of another lutjanid, *Lutjanus ehrenbergii*, averaged $\sim 0.6 \pm 0.1\%$ protein by weight, which also corroborates the low percentage composition we report herein (McMahon *et al.* 2011). Protein content for other species reported in the literature range from 0.16% to over 10% by weight, but most reported concentrations are below 3% (Degens *et al.* 1969; Morales-Nin 1986a, 1986b; Baba *et al.* 1991; Sasagawa and Mugiya 1996; Hüsey *et al.* 2004). Ontogenetic comparisons of otolith protein concentration are rare, but those in existence have found juvenile otoliths to have higher protein concentrations than those of adults (Morales-Nin 1986a, 1986b). Jolivet *et al.* (2008), likewise, showed organic fractions to be higher in otolith cores than in subsequent growth bands. We did not see this trend in red snapper otoliths. We hypothesise that the rapid otolith accretion occurring in species with large otoliths results in high mineral-to-protein ratios through all life stages, a mechanism that has been suggested to explain low protein or nitrogen content in other species with large otoliths (K. McMahon, pers. comm.; Lueders-Dumont *et al.* 2020). To our knowledge, no other studies have investigated protein concentration dynamics over continuous, multi-year time scales as a metric for age estimation.

Increasing sample mass without increasing constituent concentration can lead to a false ‘age’ effect, as was demonstrated in our CaCO_3 layer-age experiment. Because we know the composition of the CaCO_3 powder to be uniform in concentration, we can hypothesise that the wavenumbers correlated with the false ‘age’ effect resulted from the persistent carbonate ion signature coupled with changes to light absorption/penetration inherent to increasing sample mass and thickness. Although wavenumber ranges used in the ‘layer-age’ prediction models were similar to those used in the otolith age models, the specific absorbance patterns varied substantially, and the peaks associated with ‘layer age’ might

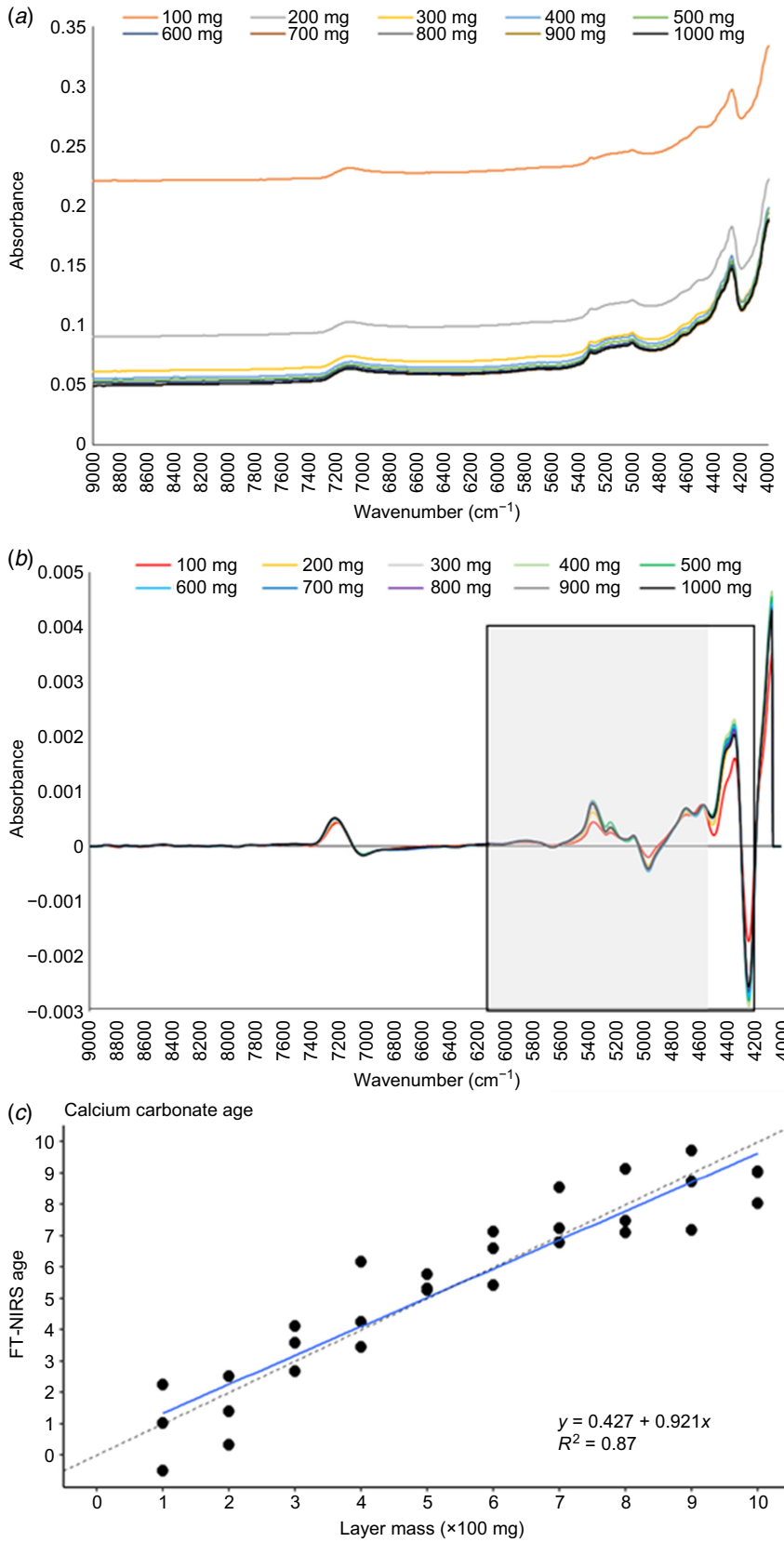


Fig. 7. Results of calcium carbonate layering experiment: (a) raw and (b) preprocessed spectral signatures by layer mass (thickness), and (c) ‘standardised’ region (6104–4200 cm⁻¹) PLS regression model results of ‘layer-age’ prediction (solid line) relative to a 1:1 relationship (dashed lines).

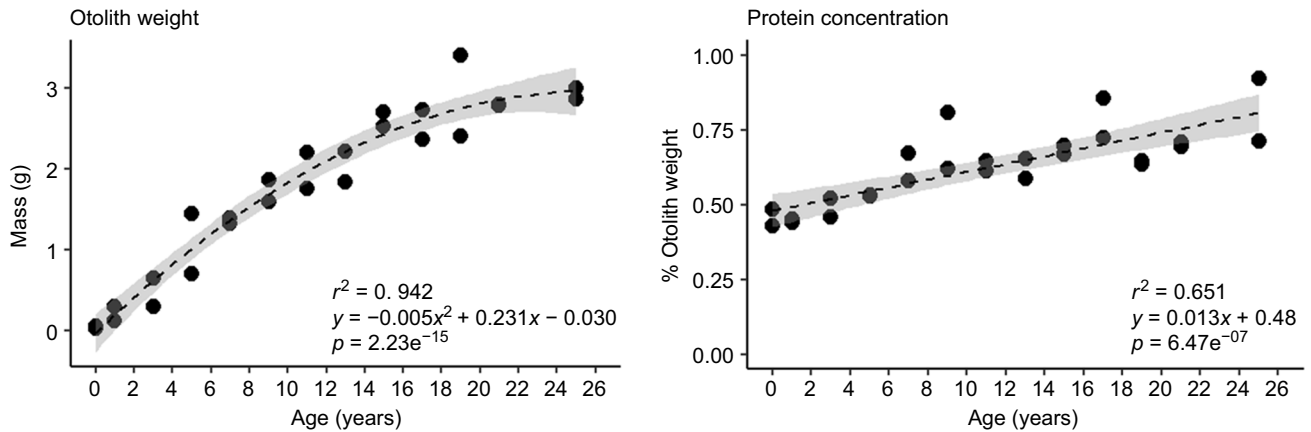


Fig. 8. Red snapper otolith weight (g) and protein concentration (% otolith weight) as a function of age, with best-fit regression lines (dashed) and 95% confidence intervals (grey) plotted.

simply correspond to the molecular bonds present in CaCO_3 that are most sensitive to changes in light penetration with an increasing layer thickness, similar to the limitations of light penetration documented in [Passerotti et al. \(2020b\)](#).

Other physical considerations are apparent when age-prediction capability is compared in ground and intact otoliths. Altering the sample structure and presentation of whole intact otoliths by grinding them reduced explained variance by $\sim 6\%$ and increased model error by $\sim 40\%$ in standardised models, but did not inhibit age-prediction capability completely. Further, in both whole ground and FMG samples, the age prediction regression became more non-linear with grinding and subsampling respectively. This suggests that the ordered structure of whole otoliths and the associated layered growth pattern is more conducive to linear age-prediction modelling than are homogenised samples, which is contrary to most reported effects of grinding on NIRS prediction (e.g. wheat kernels; [Williams 2019](#)). One potential explanation for this observation is the spatial heterogeneity of protein distribution documented in otoliths owing to the precipitation of otolith material from the saccular epithelium. Concentration gradients are present in the otolith cavity, which result in higher constituent concentrations, namely proteins, in areas in close contact with epithelium (e.g. [Payan et al. 1999](#)). The otolith sulcus is generally the site in direct contact with the cells responsible for deposition of protein matrix onto the surface of the accreting otolith ([Dunkelberger et al. 1980](#)) and collagen concentration is also highest along the sulcus ([Murayama et al. 2004](#)). Coincidentally, the sulcal face (convex side) of the otolith is the focal point for scanning in all studies conducted, based on the recommendation of [Robins et al. \(2015\)](#), which may improve age prediction relative to that of other sample presentations because of the closer proximity of integrated proteins to the NIR light. Otolith chemical gradients can also reflect the composition of the endolymph at specific points in time owing to entrapment of

endolymph in interstitial spaces during otolith mineralisation ([Thomas et al. 2019](#); [Lueders-Dumont et al. 2020](#)) and, hence, might reflect age-specific trends that also vary with habitat, diet, or physiology, because these factors influence the composition of endolymph as well ([Thomas et al. 2017](#)). In ground otoliths, the model cannot incorporate variation owing to size, shape, or layering structure so as to improve the prediction. Even with corrective preprocessing, there can still be variation owing to pathlength (the distance the light travels through the sample) incorporated into the model, as was evidenced by the ‘layer-age’ experiment, which might contribute to better NIRS age prediction in whole samples because of the effect of otolith size and thickness. Ostensibly, attenuation might occur even over small ranges of otolith size because of differences in density, opacity, and layering of the structure (e.g. [Hüssy et al. 2004](#)). Particle-size and light-scatter effects are generally reduced in ground relative to whole grains and seeds ([Williams 2019](#)), and the same is apparent in red snapper otoliths. Overall, the assumption that the behaviour of light is uniform as it passes through inherently heterogeneous otoliths must be rejected, and acknowledgement made of the physical effects surrounding FT-NIRS analysis of otoliths. Additionally, non-linear spectral modelling techniques should be explored for improved age prediction given the possibility that age-related constituent changes are better described with non-linear relationships.

The spectral region $4688\text{--}4544\text{ cm}^{-1}$, which is known to be associated with protein discrimination in a range of other NIRS applications ([Workman and Weyer 2012](#)), was used to inform the optimised age-prediction model for FMG samples but was not included in whole otolith optimised age models. This might seem to discount previously published theories e.g. [Helser et al. \(2019\)](#) that FT-NIRS age models reflect changes in protein concentration with age; however, this is not necessarily the case. Vibrational modes are harmonic; hence, the impact of one type of bond vibration will appear

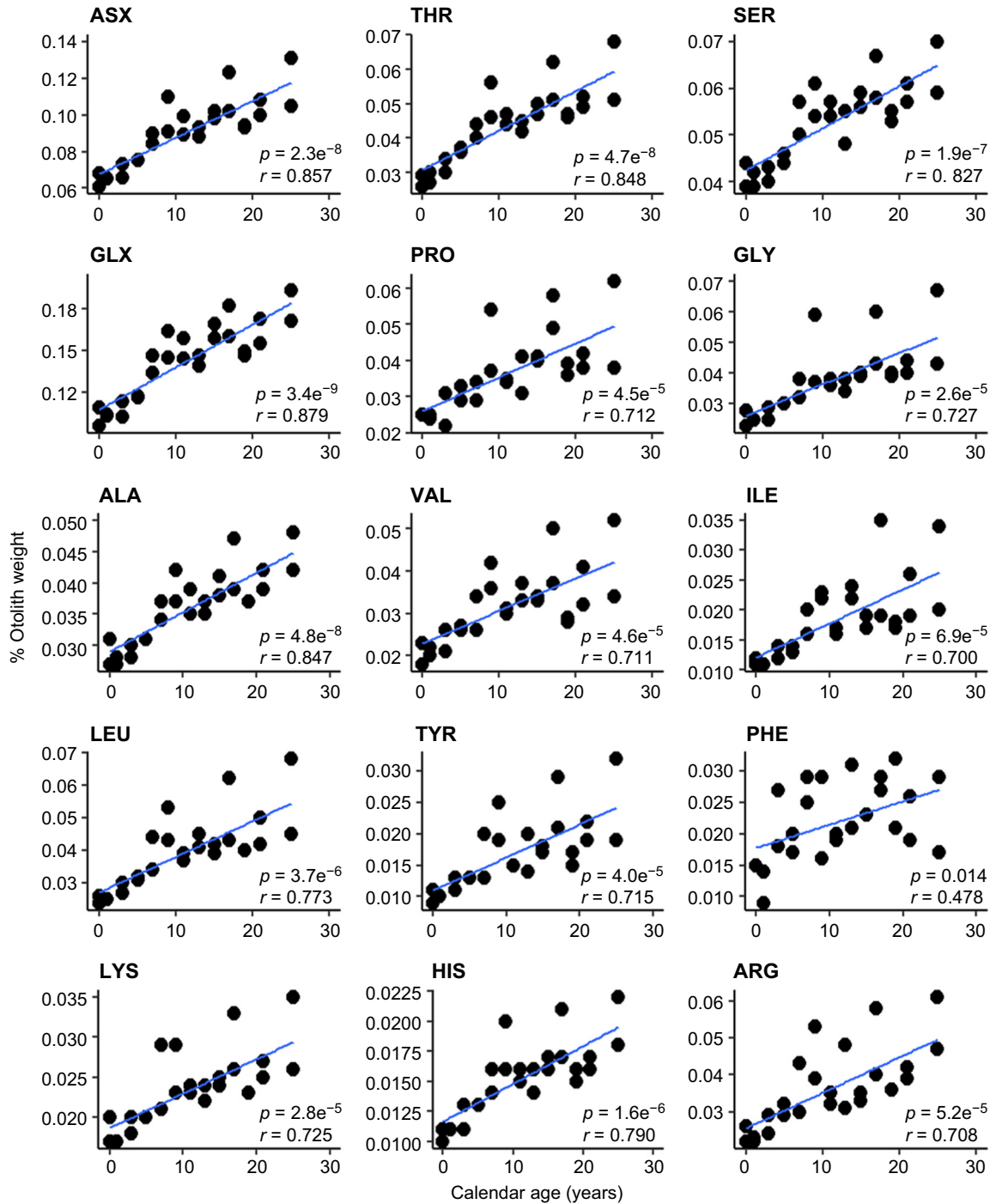


Fig. 9. Red snapper otolith amino acid concentrations (% otolith weight) for aspartic acid/asparagine (ASX), threonine (THR), serine (SER), glutamic acid/glutamine (GLX), proline (PRO), glycine (GLY), alanine (ALA), valine (VAL), isoleucine (ILE), leucine (LEU), tyrosine (TYR), phenylalanine (PHE), lysine (LYS), histidine (HIS), and arginine (ARG) plotted by age (traditional otolith age in years). Correlation coefficients and significance are given for each regression.

at multiple points in the NIR spectrum, primarily as combination bands in the lower wavenumber regions and again as overtones at higher wavenumbers. Proteins and peptides (detected in NIR spectra using their amide content) can be detected in other regions including 10 277–

9804 cm^{-1} , 6667–6536 cm^{-1} , 4878–4854 cm^{-1} and 4400–4000 cm^{-1} (Workman and Weyer 2012). Hence, exclusion of a specific wavenumber from a model does not mean other corresponding molecular vibrations are not present elsewhere in the signature. The 4688–4544 cm^{-1} region

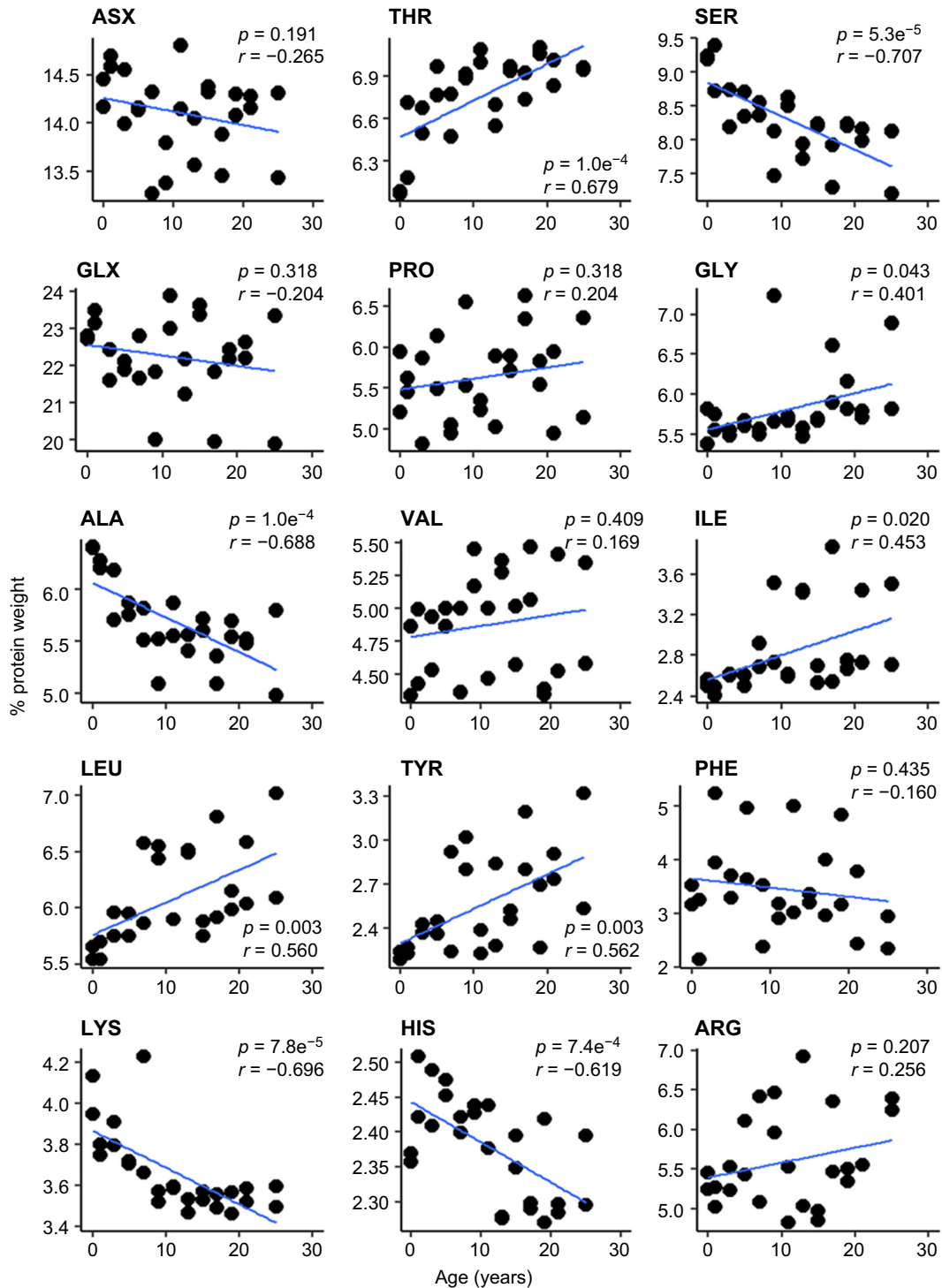


Fig. 10. Red snapper otolith amino acid concentration (% total protein weight), for aspartic acid/asparagine (ASX), threonine (THR), serine (SER), glutamic acid/glutamine (GLX), proline (PRO), glycine (GLY), alanine (ALA), valine (VAL), isoleucine (ILE), leucine (LEU), tyrosine (TYR), phenylalanine (PHE), lysine (LYS), histidine (HIS), and arginine (ARG) plotted by age (traditional otolith age in years). Correlation coefficients and significance are given for each regression.

Table 2. Outcomes from FT-NIRS prediction of red snapper otolith protein concentration (percentage otolith weight) using PLS regression models.

Model	n	Wavenumber region(s)	R ²	RMSECV	RPD	Bias	Rank
Intact protein, standardised	26	6104–4200	59.9	0.078	1.58	8.3e–5	2
Intact protein, optimised	26	7456–6768 6400–6024	67.9	0.070	1.76	1.3e–4	2
Intact protein reduced, optimised	23	4688–4600	86.3	0.035	2.7	5.0e–4	2
Fixed-mass ground protein, standardised	21	6104–4200	30.9	0.083	1.2	8.6e–4	1
Fixed-mass ground protein, optimised	21	6032–5496	52.9	0.069	1.46	4.0e–3	8
Fixed-mass ground protein reduced, optimised	18	4600–4544	90.5	0.019	3.25	8.1e–5	5

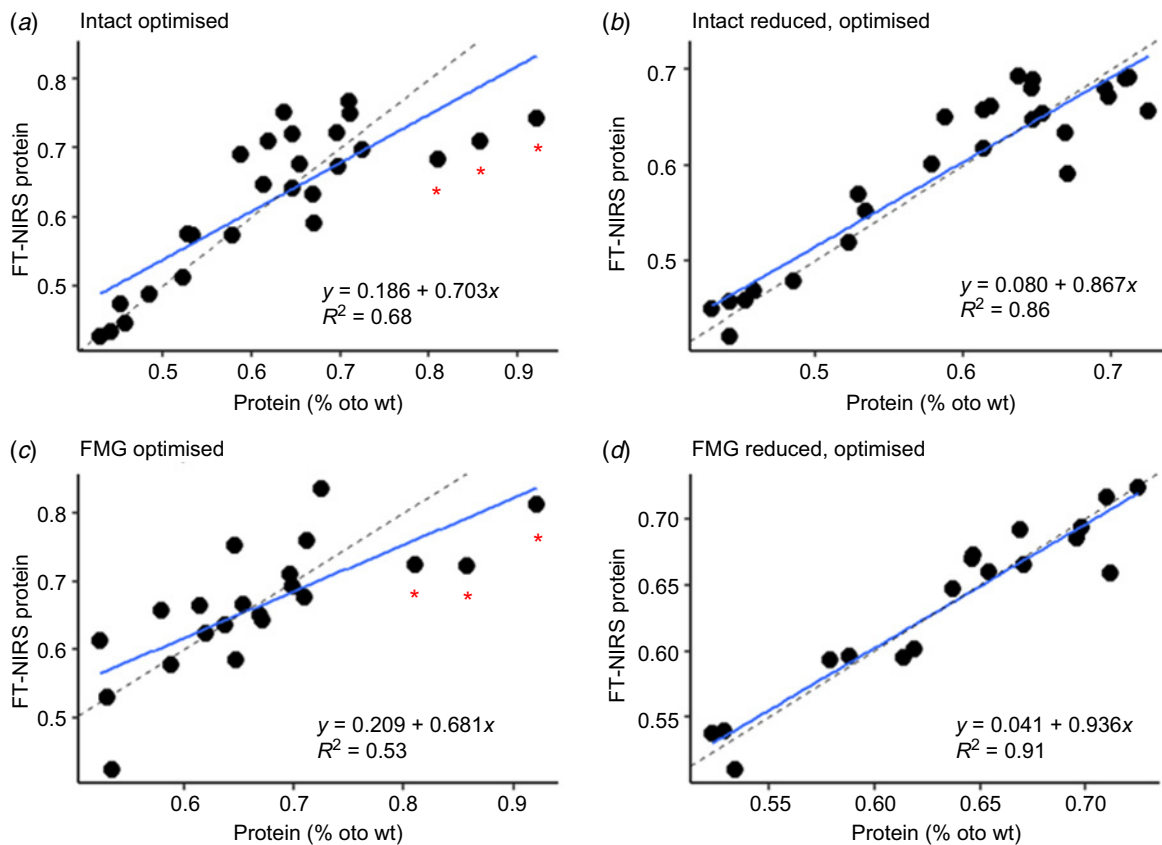


Fig. 11. Red snapper otolith protein PLS regression model results for FT-NIRS predicted protein concentration (solid lines) relative to a 1:1 relationship (dashed lines) on the basis of spectra from (a) whole intact, (b) whole intact minus outliers (reduced), (c) fixed-mass ground (FMG) and (d) FMG minus outliers sample sets. Concentration outliers that were removed for "reduced" models are denoted in a and c with red asterisks.

reflects C–H, C=O, C–N and N–H bonds, all of which are present in protein molecules. Overtones of C–H vibrations appear between 6030 and 5500 cm⁻¹, followed by N–H overtones between 6770 and 6030 cm⁻¹ (Workman and Weyer 2012), and both of these regions are included in whole otolith optimised age models. Additionally, the age-correlated decrease in mineral fraction that ostensibly happens concurrent to the increasing organic fraction is itself measurable and might produce a more easily detectable

and less variable signal than do organic components because of the higher percentage composition of CaCO₃. This type of correlation, in which a characteristic is measured via the change in an associated but more easily measured constituent, is commonly used in NIRS analyses (Williams 2019). Hence, the effect of changing protein content on age prediction is captured at multiple points throughout the spectral signature, and at wavenumber regions associated with both protein and carbonate molecules, an argument that is supported by our

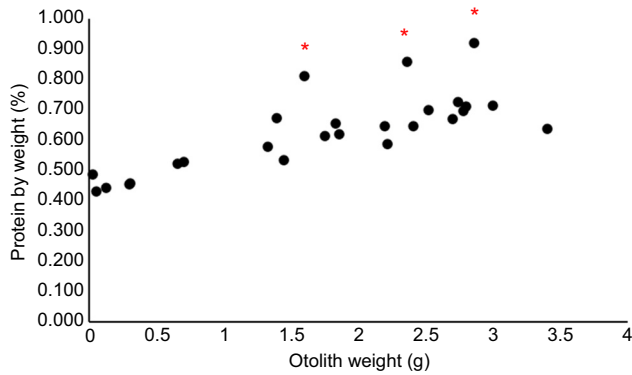


Fig. 12. Red snapper otolith protein concentration (% otolith weight) plotted as a function of otolith weight. Samples indicated by red asterisks were identified as outliers in protein prediction PLS regression models and were removed to produce “reduced” protein-prediction models.

analysis of age model regression coefficients, using carbonate and collagen-associated wavenumbers. As such, both the magnitude and direction of correlation are important when evaluating the influence of wavenumber regions on age models.

Age-related trends in amino acid concentrations relative to total protein weight suggest that the composition of otolith proteins varies significantly across the lifespan of red snapper, which has manifold impacts on how spectral signatures of otoliths change with age. Amino acids contain characteristic amide groups in varying quantities and molecular configurations and, in addition to the overall quantity of bonds, their positioning within the amino acid structure as well as protein folding patterns affect the molecular architecture and thus bond-vibration characteristics (Czarnecki *et al.* 2015; Williams 2019). Hence, specific amino acid and thus protein composition as a whole affect the corresponding spectral signature. Otolith protein composition changes with age and species-specific patterns in otolith amino acid composition have also been documented (Söllner *et al.* 2003; Tohse *et al.* 2008; Weigele *et al.* 2016; Lueders-Dumont *et al.* 2020). Without knowing the specific proteins contained in red snapper otoliths, it is difficult to interpret specific effects on the otolith spectral signature and overall age prediction. These findings have impacts on the future use of FT-NIRS not only for age prediction, but also to infer habitat and life history-related information from otolith signatures. Otolith chemistry is widely utilised in ecological studies to reconstruct migration, habitat use, and diet via the chronologically ordered recording of trace element and isotopic profiles within the otolith (e.g. Elsdon *et al.* 2008; Walther 2019). Future studies examining the ability of FT-NIRS to reflect fine-scale otolith protein dynamics would be beneficial in the pursuit of a less-expensive and non-destructive method of discriminating otolith chemistry for application to broader fisheries management goals.

Conclusions

Near-infrared spectroscopy in otoliths shows potential for application to a wide range of fisheries research areas, including age estimation. However, the realisation of its potential will progress only as fast as our understanding of otolith compositional dynamics, which act alongside otolith morphometrics to drive NIRS spectral signatures. In-depth holistic studies of otolith compositional dynamics are rare, but recent advances in high-resolution detection and visualisation of key constituents (e.g. Thomas *et al.* 2019, 2020; Hüsey *et al.* 2021a) highlight their usefulness. Otoliths are increasingly used as fine-scale chemical chronometers to reconstruct environmental and metabolic histories; NIRS could be a transformative tool in these pursuits, but the integrative nature of physical and chemical properties inherent to NIRS analysis cannot be disregarded.

Supplementary material

Supplementary material is available [online](#).

References

- Alm E, Bro R, Engelsen SB, Karlberg B, Torgrip RJO (2007) Vibrational overtone combination spectroscopy (VOCSY) – a new way of using IR and NIR data. *Analytical and Bioanalytical Chemistry* **388**, 179–188. doi:10.1007/s00216-007-1180-8
- Baba K, Shimizu M, Mugiya Y, Yamada J (1991) Otolith matrix proteins of walleye pollock; biochemical properties and immunohistochemical localization in the saccular tissue. In ‘Mechanisms and phylogeny of mineralization in biological systems’. (Eds S Suga, H Nakahara) pp. 57–61. (Springer Japan: Tokyo, Japan) doi:10.1007/978-4-431-68132-8_9
- Beebe KR, Pell RJ, Seasholtz MB (1998) ‘Chemometrics: a practical guide (Vol. 4)’, (Wiley: New York, NY, USA)
- Borelli G, Mayer-Gostan N, De Pontual H, Boeuf G, Payan P (2001) Biochemical relationships between endolymph and otolith matrix in the trout (*Oncorhynchus mykiss*) and turbot (*Psetta maxima*). *Calcified Tissue International* **69**, 356–364. doi:10.1007/s00223-001-2016-8
- Campana S (1999) Chemistry and composition of fish otoliths: pathways, mechanisms and applications. *Marine Ecology Progress Series* **188**, 263–297. doi:10.3354/meps188263
- Campana SE (2001) Accuracy, precision and quality control in age determination, including a review of the use and abuse of age validation methods. *Journal of Fish Biology* **59**, 197–242. doi:10.1111/j.1095-8649.2001.tb00127.x
- Chang M-Y, Geffen AJ (2013) Taxonomic and geographic influences on fish otolith microchemistry. *Fish and Fisheries* **14**, 458–492. doi:10.1111/j.1467-2979.2012.00482.x
- Chen J, Wang XZ (2001) A new approach to near-infrared spectral data analysis using independent component analysis. *Journal of Chemical Information and Computer Sciences* **41**(4), 992–1001.
- Cooper C, Packer N, Williams K (2000). ‘Amino acid analysis protocols’, (Humana Press) doi:10.1385/1592590470
- Czarnecki MA, Morisawa Y, Futami Y, Ozaki Y (2015) Advances in molecular structure and interaction studies using near-infrared spectroscopy. *Chemical Reviews* **115**, 9707–9744. doi:10.1021/cr500013u
- Dauphin Y, Dufour E (2003) Composition and properties of the soluble organic matrix of the otolith of a marine fish: *Gadus morhua* Linne, 1758 (Teleostei, Gadidae). *Comparative Biochemistry and Physiology – A*.

- Molecular & Integrative Physiology* **134**, 551–561. doi:10.1016/S1095-6433(02)00358-6
- Davis J, Oberholtzer JC, Burns FR, Greene MI (1995) Molecular cloning and characterization of an inner ear-specific structural protein. *Science* **267**, 1031–1034. doi:10.1126/science.7863331
- Degens ET, Deuser WG, Haedrich RL (1969) Molecular structure and composition of fish otoliths. *Marine Biology* **2**(2), 105–113. doi:10.1007/BF00347005
- Dunkelberger DG, Dean JM, Watabe N (1980) The ultrastructure of the otolithic membrane and otolith in the juvenile mummichog, *Fundulus heteroclitus*. *Journal of Morphology* **163**, 367–377. doi:10.1002/jmor.1051630309
- Elsdon TS, Wells BK, Campana SE, Gillanders BM, Jones CM, Limburg KE, Secor DH, Thorrold SR, Walther BD (2008) Otolith chemistry to describe movements and life-history parameters of fishes: hypotheses, assumptions, limitations and inferences. In 'Oceanography and marine biology – an annual review'. Vol. 46. (Eds RN Gibson, RJA Atkinson, JDM Gordon) pp. 297–330. (Taylor & Francis) doi:10.1201/9781420065756.ch7
- Gaffey SJ (1987) Spectral reflectance of carbonate minerals in the visible and near infrared (0.35–2.55 μm): anhydrous carbonate minerals. *Journal of Geophysical Research – Solid Earth* **92**, 1429–1440. doi:10.1029/JB092iB02p01429
- Gauldie RW, Thacker CE, West IF, Wang L (1998) Movement of water in fish otoliths. *Comparative Biochemistry and Physiology Part A. Molecular & Integrative Physiology* **120**, 551–556. doi:10.1016/S1095-6433(98)10065-X
- Healy J, Helser TE, Benson IM, Tornabene L (2021) Aging Pacific cod (*Gadus macrocephalus*) from otoliths using Fourier-transformed near-infrared spectroscopy. *Ecosphere* **12**(8), e03697.
- Helser TE, Benson I, Erickson J, Healy J, Kastle JA (2019) A transformative approach to ageing fish otoliths using Fourier transform near infrared spectroscopy: a case study of eastern Bering Sea walleye pollock (*Gadus chalcogrammus*). *Canadian Journal of Fisheries and Aquatic Sciences* **76**, 780–789. doi:10.1139/cjfas-2018-0112
- Hoff GR, Fuiman LA (1993) Morphometry and composition of red drum otoliths: changes associated with temperature, somatic growth rate, and age. *Comparative Biochemistry and Physiology Part A: Physiology* **106**, 209–219. doi:10.1016/0300-9629(93)90502-U
- Hopkinson L, Rutt KJ (2016) Crystal chemical correlations between the mid and near-infrared in carbonate minerals. *Spectrochimica Acta Part A: Molecular and Biomolecular Spectroscopy* **162**, 105–108. doi:10.1016/j.saa.2016.03.004
- Hopkinson L, Kristova P, Rutt K (2017) The near-infrared (NIR) spectra of powdered calcite in the 3–121 μm mode particle size range. *Vibrational Spectroscopy* **90**, 69–73. doi:10.1016/j.vibspec.2017.03.006
- Hüssy K, Mosegaard H, Jessen F (2004) Effect of age and temperature on amino acid composition and the content of different protein types of juvenile Atlantic cod (*Gadus morhua*) otoliths. *Canadian Journal of Fisheries and Aquatic Sciences* **61**, 1012–1020. doi:10.1139/f04-037
- Hüssy K, Krüger-Johnsen M, Thomsen TB, Heredia BD, Naeraa T, Limburg KE, Heimbrand Y, McQueen K, Haase S, Krumme U, Casini M, Mion M, Radtke K (2021a) It's elemental, my dear Watson: validating seasonal patterns in otolith chemical chronologies. *Canadian Journal of Fisheries and Aquatic Sciences* **78**(5), 551–566. doi:10.1139/cjfas-2020-0388
- Hüssy K, Limburg KE, de Pontual H, Thomas ORB, Cook PK, Heimbrand Y, Blass M, Sturrock AM (2021b) Trace element patterns in otoliths: the role of biomineralization. *Reviews in Fisheries Science & Aquaculture* **29**, 445–477. doi:10.1080/23308249.2020.1760204
- Izzo C, Doubleday ZA, Gillanders BM (2016) Where do elements bind within the otoliths of fish? *Marine and Freshwater Research* **67**, 1072–1076. doi:10.1071/MF15064
- Jolivet A, Bardeau J-F, Fablet R, Paulet Y-M, de Pontual H (2008) Understanding otolith biomineralization processes: new insights into microscale spatial distribution of organic and mineral fractions from Raman microspectrometry. *Analytical and Bioanalytical Chemistry* **392**, 551–560. doi:10.1007/s00216-008-2273-8
- Jolivet A, Bardeau J-F, Fablet R, Paulet Y-M, de Pontual H (2013) How do the organic and mineral fractions drive the opacity of fish otoliths? Insights using Raman microspectrometry. *Canadian Journal of Fisheries and Aquatic Sciences* **70**, 711–719. doi:10.1139/cjfas-2012-0298
- Kandel S, Querido W, Falcon JM, Reiners DJ, Pleshko N (2020) Approaches for *in situ* monitoring of matrix development in hydrogel-based engineered cartilage. *Tissue Engineering Part C: Methods* **26**, 225–238. doi:10.1089/ten.tec.2020.0014
- Limburg KE, Elfman M (2017) Insights from two-dimensional mapping of otolith chemistry: otolith chemical mapping. *Journal of Fish Biology* **90**, 480–491. doi:10.1111/jfb.13048
- Lueders-Dumont JA, Sigman DM, Johnson BJ, Jensen OP, Oleynik S, Ward BB (2020) Comparison of the isotopic composition of fish otolith-bound organic N with host tissue. *Canadian Journal of Fisheries and Aquatic Sciences* **77**, 264–275. doi:10.1139/cjfas-2018-0360
- McMahon KW, Berumen ML, Mateo I, Elsdon TS, Thorrold SR (2011) Carbon isotopes in otolith amino acids identify residency of juvenile snapper (Family: Lutjanidae) in coastal nurseries. *Coral Reefs* **30**, 1135–1145. doi:10.1007/s00338-011-0816-5
- Morales-Nin B (1986a) Chemical composition of the otoliths of the sea bass (*Dicentrarchus labrax* Linnaeus, 1758) (Pisces, Serranidae). *Cybiurn* **10**, 115–120.
- Morales-Nin B (1986b) Structure and composition of otoliths of Cape hake *Merluccius capensis*. *South African Journal of Marine Science* **4**, 3–10. doi:10.2989/025776186784461639
- Murayama E, Takagi Y, Ohira T, Davis JG, Greene MI, Nagasawa H (2002) Fish otolith contains a unique structural protein, otolin-1. *European Journal of Biochemistry* **269**, 688–696. doi:10.1046/j.0014-2956.2001.02701.x
- Murayama E, Takagi Y, Nagasawa H (2004) Immunohistochemical localization of two otolith matrix proteins in the otolith and inner ear of the rainbow trout, *Oncorhynchus mykiss*: comparative aspects between the adult inner ear and embryonic otocysts. *Histochemistry and Cell Biology* **121**, 155–166. doi:10.1007/s00418-003-0605-5
- Passerotti MS, Helser TE, Benson IM, Barnett BK, Ballenger JC, Bublely WJ, Reichert MJM, Quattro JM (2020a) Age estimation of red snapper (*Lutjanus campechanus*) using FT-NIR spectroscopy: feasibility of application to production ageing for management. *ICES Journal of Marine Science* **77**, 2144–2156. doi:10.1093/icesjms/fsaa131
- Passerotti MS, Jones CM, Swanson CE, Quattro JM (2020b) Fourier-transform near infrared spectroscopy (FT-NIRS) rapidly and non-destructively predicts daily age and growth in otoliths of juvenile red snapper *Lutjanus campechanus* (Poey, 1860). *Fisheries Research* **223**, 105439. doi:10.1016/j.fishres.2019.105439
- Payan P, Edeyer A, de Pontual H, Borelli G, Boeuf G, Mayer-Gostan N (1999) Chemical composition of saccular endolymph and otolith in fish inner ear: lack of spatial uniformity. *American Journal of Physiology. Regulatory, Integrative and Comparative Physiology* **277**, R123–R131. doi:10.1152/ajpregu.1999.277.1.R123
- Rigby CL, Wedding BB, Grauf S, Simpfendorfer CA (2014) The utility of near infrared spectroscopy for age estimation of deepwater sharks. *Deep-sea Research – I. Oceanographic Research Papers* **94**, 184–194. doi:10.1016/j.dsr.2014.09.004
- Rigby CL, Wedding BB, Grauf S, Simpfendorfer CA (2016) Novel method for shark age estimation using near infrared spectroscopy. *Marine and Freshwater Research* **67**, 537–545. doi:10.1071/MF15104
- Rigby CL, Foley WJ, Simpfendorfer CA (2019) Near-infrared spectroscopy for shark ageing and biology. In 'Shark research: emerging technologies and applications for the field and laboratory'. (Eds JC Carrier, MR Heithaus, CA Simpfendorfer) pp. 201–218. (CRC Press)
- Rinnan Å, van den Berg F, Engelsen SB (2009) Review of the most common pre-processing techniques for near-infrared spectra. *Trends in Analytical Chemistry* **28**, 1201–1222. doi:10.1016/j.trac.2009.07.007
- Robins J, Wedding BB, Wright C, Grauf S, Sellin M, Fowler A, Saunders T, Newman S (2015). 'Revolutionising fish ageing: using near infrared spectroscopy to age fish', (Fisheries Research & Development Corporation (Australia), Department of Agriculture and Fisheries: Qld, Australia)
- Sasagawa T, Mugiya Y (1996) Biochemical properties of water-soluble otolith proteins and the immunobiochemical detection of the proteins in serum and various tissues in the tilapia *Oreochromis niloticus*. *Fisheries Science* **62**, 970–976. doi:10.2331/fishsci.62.970
- Siesler HW, Ozaki Y, Kawata S, Heise HM (2002). 'Near-infrared spectroscopy: principles, instruments, applications', (Wiley)
- Söllner C, Burghammer M, Busch-Nentwich E, Berger J, Schwarz H, Riekel C, Nicolson T (2003) Control of crystal size and lattice formation by

- Starmaker in otolith biomineralization. *Science* **302**, 282–286. doi:10.1126/science.1088443
- Thomas ORB, Swearer SE (2019) Otolith biochemistry – a review. *Reviews in Fisheries Science & Aquaculture* **27**, 458–489. doi:10.1080/23308249.2019.1627285
- Thomas ORB, Ganio K, Roberts BR, Swearer SE (2017) Trace element–protein interactions in endolymph from the inner ear of fish: implications for environmental reconstructions using fish otolith chemistry. *Metallomics* **9**, 239–249. doi:10.1039/C6MT00189K
- Thomas ORB, Swearer SE, Kapp EA, Peng P, Tonkin-Hill GQ, Papenfuss A, Roberts A, Bernard P, Roberts BR (2019) The inner ear proteome of fish. *The FEBS Journal* **286**, 66–81. doi:10.1111/febs.14715
- Thomas ORB, Richards KL, Petrou S, Roberts BR, Swearer SE (2020) In situ 3D visualization of biomineralization matrix proteins. *Journal of Structural Biology* **209**, 107448. doi:10.1016/j.jsb.2020.107448
- Tohse H, Takagi Y, Nagasawa H (2008) Identification of a novel matrix protein contained in a protein aggregate associated with collagen in fish otoliths. *FEBS Journal* **275**, 2512–2523. doi:10.1111/j.1742-4658.2008.06400.x
- Walther BD (2019) The art of otolith chemistry: interpreting patterns by integrating perspectives. *Marine and Freshwater Research* **70**, 1643–1658. doi:10.1071/MF18270
- Wedding BB, Forrest AJ, Wright C, Grauf S, Exley P, Poole SE (2014). A novel method for the age estimation of saddletail snapper (*Lutjanus malabaricus*) using Fourier transform-near infrared (FT-NIR) spectroscopy. *Marine and Freshwater Research* **65**, 894. doi:10.1071/MF13244
- Weigele J, Franz-Odenaal TA, Hilbig R (2016) Not all inner ears are the same: otolith matrix proteins in the inner ear of sub-adult cichlid fish, *Oreochromis mossambicus*, reveal insights into the biomineralization process: otolith matrix proteins in cichlid fish. *The Anatomical Record* **299**, 234–245. doi:10.1002/ar.23289
- Williams P (2013) Calibration development and evaluation methods B. Set-Up and evaluation. *NIR News* **24**(6), 20–24.
- Williams P (2019) ‘Near infrared technology: getting the best out of light.’ (AFRICAN SUN MeDIA)
- Williams PC, Norris KH, Sobering DC (1985) Determination of protein and moisture in wheat and barley by near-infrared transmission. *Journal of Agricultural and Food Chemistry* **33**, 239–244. doi:10.1021/jf00062a021
- Workman JJ Jr (2001) Infrared and raman spectroscopy in paper and pulp analysis. *Applied Spectroscopy Reviews* **36**, 139–168. doi:10.1081/ASR-100106154
- Workman J Jr, Weyer L (2012) ‘Practical guide and spectral atlas for interpretive near-infrared spectroscopy’, 2nd edn. (CRC Press)
- Wright C, Wedding BB, Grauf S, Whybird OJ (2021) Age estimation of barramundi (*Lates calcarifer*) over multiple seasons from the southern Gulf of Carpentaria using FT-NIR spectroscopy. *Marine and Freshwater Research* **72**(9), 1268–1279.
- Wyanski D, White DB, Smart T, Kolmos K, Reichert MJ (2015) Marine resources monitoring, assessment and prediction program: report on Atlantic red snapper, *Lutjanus campechanus*, life history for the SEDAR 41 Data Workshop SEDAR41–DW35. SEDAR, North Charleston, SC, USA.

Data availability. The data underlying this article will be shared on reasonable request to the corresponding author.

Conflicts of interest. The authors declare that they have no conflicts of interest.

Declaration of funding. This work was supported by South Carolina Sea Grant [R/CF-23], an equipment grant from the College of Arts and Sciences, University of South Carolina, and funds from a SPARC Graduate Research and an ASPIRE-I grant from the Office of the Vice President for Research at the University of South Carolina. Z. M. was supported by the National Science Foundation EPSCoR Program under NSF Award #OIA-1655740.

Acknowledgements. The authors thank the staff at the SC DNR Marine Resources Research Institute for providing otoliths and age and other meristic data for this study, especially D. B. White, J. Evans, W. Bublely, J. Ballenger, and M. Willis. We thank G. Yagodzinski, J. Weeks, N. Earl, K. Levasseur, and K. Fuller of University of South Carolina for assistance with experiments. This work made use of the South Carolina SAXS Collaborative (SCSC). N. Pleshko and S. Kandel (Temple University, Philadelphia, PA, USA) kindly provided data on collagen NIR signatures that were key to the success of the study. M. Myrick was instrumental in providing insights and guidance on experimental design and interpretation. C. Rigby provided invaluable discussion and advice over several years regarding otolith/vertebral chemistry and their relationship to FT-NIRS. We also thank J. Erickson for providing expertise on FT-NIRS equipment and experimental design. This is contribution # 849 of SCDNR’s Marine Resources Research Institute. The findings and conclusions in the paper are those of the author(s) and do not necessarily represent the views of the National Marine Fisheries Service.

Author affiliations

^ADepartment of Biological Sciences, University of South Carolina, Columbia, SC 29208, USA.

^BPresent address: NOAA Fisheries Apex Predators Program, 28 Tarzwell Drive, Narragansett, RI 02884, USA.

^CSouth Carolina Department of Natural Resources, Marine Resources Research Institute, Charleston, SC 29412, USA.

^DPresent address: Department of Natural Resources Management, Texas Tech University, Lubbock, TX 79409, USA.

^EDepartment of Chemistry and Biochemistry, University of South Carolina, Columbia, SC 29208, USA.

^FSchool of the Earth, Ocean, and Environment, University of South Carolina, Columbia, SC 29208, USA.